Stability Analysis of Turning With Periodic Spindle Speed Modulation Via Semidiscretization

TAMÁS INSPERGER
GÁBOR STÉPÁN
Department of Applied Mechanics, Budapest University of Technology and Economics, Budapest, H-1521, Hungary

(Received 25 November 2003; accepted 12 March 2004)

Abstract: We investigate a single-degree-of-freedom model of turning with sinusoidal spindle speed modulation and the corresponding delay-differential equation with time-varying delay. The equation is analyzed by the numerical semidiscretization method. Stability charts and chatter frequencies are constructed. Improvement in the efficiency of machining is found for high modulation frequency and for low spindle speed domain. Period-one, period-two (flip), and secondary Hopf bifurcations were detected by eigenvalue analysis.

Key Words: Turning, chatter, varying spindle speed, time-dependent time delay

1. INTRODUCTION

Systems governed by delay-differential equations (DDEs) often appear in different fields of science and engineering. One of the most important mechanical applications is the cutting process dynamics. As a result of the extensive work of Tlusty et al. (1962), Tobias (1965), and Kudinov (1967), the so-called regenerative effect has become the most commonly accepted explanation for machine tool chatter (Stépán, 1989; Moon, 1998). This effect is related to the cutting force variation due to the wavy workpiece surface cut in the preceding revolution. The corresponding mathematical models are DDEs associated with infinite-dimensional state spaces. For the case of turning, the delay is equal to the rotation period of the workpiece, while for milling it is equal to the tooth passing period. Consequently, if the spindle speed is constant in time, then the delay is also constant, and the governing equation is a DDE with constant delay (CDDE). Several techniques exist for analyzing CDDEs and predicting stability behavior for cutting processes with constant spindle speeds (see, for example, Altintas et al., 1999; Segalman and Butcher, 2000; Zhao and Balachandran, 2001; Gouskov et al., 2002; Bayly et al., 2003; Insperger et al., 2003; Szalai and Stépán, 2003). For cutting processes, the stability properties are presented in the so-called stability charts, which plot the maximum chatter-free chip width as a function of spindle speed.

The identification of the arising vibrations during machining can effectively be supported by the frequency analysis of chatter signals (Gradišek et al., 2002; Schmitz et al., 2002). The stability charts published in the specialist literature are almost always accompanied by

Journal of Vibration and Control, **10:** 1835–1855, 2004 DOI: 10.1177/1077546304044891

frequency diagrams that represent the chatter frequencies at the loss of stability (Insperger et al., 2003). The reason for this custom is that these frequencies can precisely be identified experimentally and so this is a direct way to verify theoretical models and predictions (Mann et al., 2003).

Prevention of chatter is a primary problem for machining. The idea that parametric excitation effects may suppress vibrations during the cutting process comes from the famous problem of stabilizing inverted pendulums by parametric excitation (Insperger and Horváth, 2000).

Periodically varying stiffness was suggested by Segalman and Butcher (2000) to suppress chatter in turning. They investigated the resulting DDE with time periodic coefficients by the harmonic balance method, and found some stability improvements.

In the 1970s, it was already in the focus of research work that continuous variation of cutting speed could be used for suppressing chatter (Inamura and Sata, 1974; Takemura et al., 1974; Hosho et al., 1977; Sexton et al., 1977). The governing equation for cutting with time-varying spindle speed is a DDE with varying delay (VDDE). The stability analysis of VDDEs is not as obvious as that of the CDDEs. Sexton et al. (1977) approximated the quasi-periodic solutions of the VDDE by periodic solutions and applied the harmonic balance method to derive stability boundaries. They predicted improvements in stability properties by a factor of 10 for properly chosen parameter values. In spite of some reports on successful experiments, the stability investigations of cutting with time-varying spindle speeds were not reliable enough to present a breakthrough in this field.

Pakdemirli and Ulsoy (1997) used angle coordinate as independent variable instead of time according to Tsao et al. (1993), and obtained a CDDE with periodic coefficients. They used the perturbation technique called the method of strained parameters for stability analysis.

With their novel approach, Jayaram et al. (2000) created stability charts for turning with varying spindle speed. They used quasi-periodic trial solutions for the VDDE, combined the Fourier expansion with an expansion with respect to Bessel functions, and determined stability boundaries using the harmonic balance method. Namachchivaya and Beddini (2003) transformed the time dependency from the delay term to the coefficients, and also carried out some nonlinear analysis using the small perturbation technique.

The full-discretization technique was used by Sastry et al. (2001) for sinusoidal speed modulation and by Yilmaz et al. (2002) for random spindle speed modulation. The mathematical background for the full discretization of VDDEs (also for systems with state-dependent delays) was presented by Győri et al. (1993, 1995).

The semidiscretization method was used to obtain stability charts by Insperger et al. (2001). They showed that contrary to cutting processes with constant spindle speed, where primary or secondary Hopf and period doubling bifurcations may arise only, period-one bifurcation is also a possible route for the onset of chatter for machining with varying spindle speed.

In this paper, the semidiscretization method introduced by Insperger and Stépán (2002) is applied to VDDEs. The steps of the algorithm are presented in detail for a general linear VDDE with time periodic delay. As an example, the single-degree-of-freedom (1DOF) model of turning with varying spindle speed is investigated. Stability charts with corresponding chatter frequencies are constructed. The codes of the algorithm are also attached in the Appendix.

2. SEMIDISCRETIZATION OF VDDES

We investigate the n-dimensional linear delay differential equation:

$$\begin{aligned} \dot{\mathbf{x}}(t) &= \mathbf{A}(t)\mathbf{x}(t) + \mathbf{B}(t)\mathbf{x}(t-\tau(t)), \\ \mathbf{A}(t+T) &= \mathbf{A}(t), \quad \mathbf{B}(t+T) = \mathbf{B}(t), \quad \tau(t+T) = \tau(t). \end{aligned} \tag{1}$$

The first step of semidiscretization is the construction of the time interval discretization of $[t_i, t_{i+1}]$ with length Δt, $i = 0, 1, \ldots$ so that $T = k\Delta t$, where k is an integer that can be considered as an approximation parameter regarding the time period.

Let us define the average delay for the discretization interval $[t_i, t_{i+1}]$ as

$$\tau_i = \frac{1}{\Delta t}\int_{t_i}^{t_{i+1}} \tau(t)\mathrm{d}t. \tag{2}$$

We introduce the series of integers m_i so that

$$m_i = \mathrm{int}\left(\frac{\tau_i + \Delta t/2}{\Delta t}\right), \tag{3}$$

where int is the function that rounds positive numbers towards zero (e.g. int(5.13) = 5). Since the delay is varying periodically in time, integer m_i might be different for different discretization steps. Let us introduce the maximum value of m_i as

$$M = \max_{i=1,\ldots k}\{m_i\}. \tag{4}$$

Note that M can be considered as an approximation parameter regarding the length of the time delay.

Use the notation $\mathbf{x}(t_j) = \mathbf{x}_j$ for any integer j. In the ith interval, equation (1) can be approximated as

$$\dot{\mathbf{x}}(t) = \mathbf{A}_i\,\mathbf{x}(t) + \mathbf{B}_i\,\mathbf{x}_{\tau_i}, \tag{5}$$

where

$$\mathbf{A}_i = \frac{1}{\Delta t}\int_{t_i}^{t_{i+1}} \mathbf{A}(t)\mathrm{d}t, \quad \mathbf{B}_i = \frac{1}{\Delta t}\int_{t_i}^{t_{i+1}} \mathbf{B}(t)\mathrm{d}t, \tag{6}$$

and $\mathbf{x}_{\tau_i}$ is the following approximation of the delayed term on $[t_i, t_{i+1}]$

$$\mathbf{x}(t-\tau(t)) \approx \mathbf{x}(t-\tau_i) \approx \mathbf{x}(t_i + \Delta t/2 - \tau_i) \approx \beta_i\,\mathbf{x}_{i-m_i} + \alpha_i\,\mathbf{x}_{i-m_i+1} = \mathbf{x}_{\tau_i}, \tag{7}$$

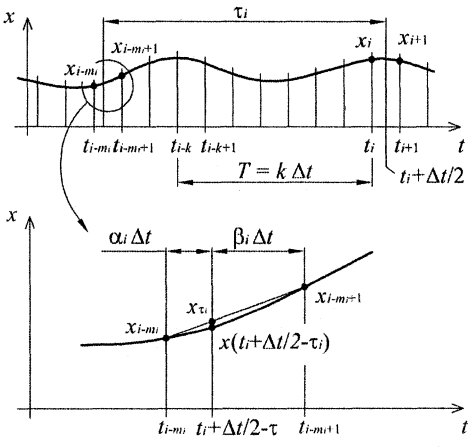

Figure 1. Approximation of the delayed term.

with weights

$$\alpha_i = \frac{m_i \Delta t + \Delta t/2 - \tau_i}{\Delta t}, \tag{8}$$

$$\beta_i = \frac{\tau_i + \Delta t/2 - m_i \Delta t}{\Delta t}. \tag{9}$$

The delayed term is approximated as a weighted linear combination of the delayed discrete values $\mathbf{x}_{i-m_i}$ and $\mathbf{x}_{i-m_i+1}$ as shown in Figure 1.

The solution of equation (5) for the initial condition

$$\mathbf{x}(t_i) = \mathbf{x}_i \tag{10}$$

reads

$$\mathbf{x}(t) = \exp\left(\mathbf{A}_i (t - t_i)\right) \left(\mathbf{x}_i + \mathbf{A}_i^{-1} \mathbf{B}_i \mathbf{x}_{\tau_i}\right) - \mathbf{A}_i^{-1} \mathbf{B}_i \mathbf{x}_{\tau_i}. \tag{11}$$

This way, $\mathbf{x}_{i+1} = \mathbf{x}(t_{i+1})$ can be expressed as

$$\mathbf{x}_{i+1} = \mathbf{P}_i \mathbf{x}_i + \alpha_i \mathbf{R}_i \mathbf{x}_{i-m_i+1} + \beta_i \mathbf{R}_i \mathbf{x}_{i-m_i}, \tag{12}$$

where

$$\mathbf{P}_i = \exp\left(\mathbf{A}_i \Delta t\right),$$
$$\mathbf{R}_i = \left(\exp\left(\mathbf{A}_i \Delta t\right) - \mathbf{I}\right) \mathbf{A}_i^{-1} \mathbf{B}_i$$

with $\mathbf{I}$ denoting the identity matrix.

Now, according to equation (12), the discrete map

$$\mathbf{y}_{i+1} = \mathbf{C}_i \mathbf{y}_i, \tag{13}$$

can be defined where the $n(M+1)$-dimensional vector is

$$\mathbf{y}_i = \mathrm{col}(\mathbf{x}_i \;\; \mathbf{x}_{i-1} \;\; \ldots \;\; \mathbf{x}_{i-M}), \tag{14}$$

and the coefficient matrix has the form

$$\mathbf{C}_i = \begin{pmatrix} \mathbf{P}_i & \mathbf{0} & \mathbf{0} & \ldots & \mathbf{0} & \alpha_i\mathbf{R}_i & \beta_i\mathbf{R}_i & \mathbf{0} & \ldots & \mathbf{0} & \mathbf{0} & \mathbf{0} \\ \mathbf{I} & \mathbf{0} & \mathbf{0} & \ldots & \mathbf{0} & \mathbf{0} & \mathbf{0} & \mathbf{0} & \ldots & \mathbf{0} & \mathbf{0} & \mathbf{0} \\ \mathbf{0} & \mathbf{I} & \mathbf{0} & \ldots & \mathbf{0} & \mathbf{0} & \mathbf{0} & \mathbf{0} & \ldots & \mathbf{0} & \mathbf{0} & \mathbf{0} \\ \vdots & \vdots & \ddots & \ddots & \vdots & \vdots & \vdots & \vdots & \vdots & \vdots & \vdots & \vdots \\ & & & & & & & & & & & \\ \vdots & \vdots & \vdots & \vdots & \vdots & \vdots & \vdots & \ddots & \ddots & \vdots & \vdots & \\ \mathbf{0} & \mathbf{0} & \mathbf{0} & \ldots & \mathbf{0} & \mathbf{0} & \mathbf{0} & \mathbf{0} & \ddots & \mathbf{0} & \mathbf{0} & \mathbf{0} \\ \mathbf{0} & \mathbf{0} & \mathbf{0} & \ldots & \mathbf{0} & \mathbf{0} & \mathbf{0} & \mathbf{0} & \ldots & \mathbf{I} & \mathbf{0} & \mathbf{0} \\ \mathbf{0} & \mathbf{0} & \mathbf{0} & \ldots & \mathbf{0} & \mathbf{0} & \mathbf{0} & \mathbf{0} & \ldots & \mathbf{0} & \mathbf{I} & \mathbf{0} \end{pmatrix}. \tag{15}$$

Here, $\alpha_i\mathbf{R}_i$ and $\beta_i\mathbf{R}_i$ are the (m_i)th and (m_i+1)th submatrices of dimension $n \times n$ in the first row of matrix $\mathbf{C}_i$.

The next step is to determine the transition matrix $\mathbf{\Phi}$ over the principal period $T = k\Delta t$. This serves a finite-dimensional approximation of the monodromy operator in the infinite-dimensional version of the Floquet theory (Hale and Lunel, 1993; Farkas, 1994). The transition matrix gives the connection between $\mathbf{y}_0$ and $\mathbf{y}_k$ in the form

$$\mathbf{y}_k = \mathbf{\Phi}\mathbf{y}_0, \tag{16}$$

where $\mathbf{\Phi}$ is given as

$$\mathbf{\Phi} = \mathbf{C}_{k-1}\mathbf{C}_{k-2}\ldots\mathbf{C}_1\mathbf{C}_0 \tag{17}$$

by coupling the solutions for each discretization interval $[t_i, t_{i+1}]$. Note that the integer k determines the number of matrices to be multiplied in equation (17), and M determines the size of these matrices.

Now, the stability investigation is reduced to the problem whether the eigenvalues of $\mathbf{\Phi}$, the so-called characteristic multipliers, are in modulus less than one (Lakshmikantham and Trigiante, 1988). At the loss of stability, the frequencies of the arising vibration are determined by the critical (greatest in modulus) characteristic multipliers.

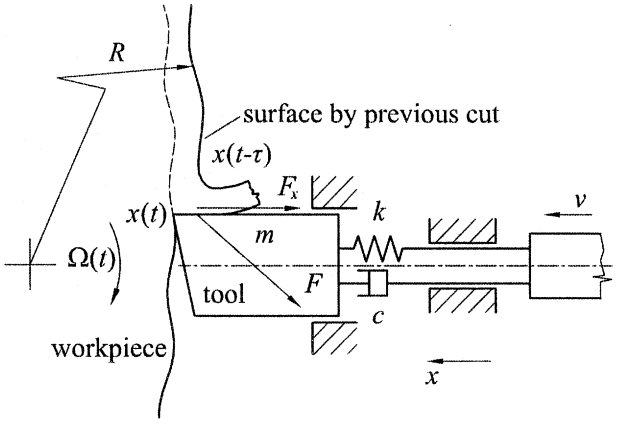

Figure 2. Mechanical model.

3. 1DOF MODEL OF TURNING WITH VARYING SPINDLE SPEED

The mechanical model of the turning process in Figure 2 is to be used with mass m, damping c, stiffness k, spindle speed $\Omega(t)$, and feed v. The linear mathematical model of chatter in turning with varying spindle speed is a T-periodic VDDE of the form

$$\ddot{x}(t) + 2\zeta\omega_n\dot{x}(t) + \omega_n^2 x(t) = -\frac{wK}{m}\left(x(t) - x(t-\tau(t))\right), \quad \tau(t+T) = \tau(t), \tag{18}$$

where $\omega_n = \sqrt{k/m}$ is the natural angular frequency, $\zeta = c/(2m\omega_n)$ is the relative damping factor of the tool, w is the depth of cut, K is the specific cutting coefficient, and the time delay $\tau(t)$ is a T-periodic function.

If the spindle speed is constant, $\Omega(t) \equiv \Omega_0$, and is given in rpm, then the time delay can be expressed as $\tau_0 = 60/\Omega_0$. In the case of time periodic spindle speed modulation $\Omega(t+T) = \Omega(t)$, the time delay is also time periodic with the same period: $\tau(t+T) = \tau(t)$. In this case, the time delay can only be given in the implicit form

$$\int_{t-\tau(t)}^{t} \Omega(s)/60\,\mathrm{d}s = 1. \tag{19}$$

This means that the workpiece makes one revolution in each time interval $[t - \tau(t), t]$ for any t.

In this paper, a sinusoidal modulation of the spindle speed is considered

$$\Omega(t) = \Omega_0 + \Omega_1\cos(\omega_m t), \tag{20}$$

where Ω_0 is the mean value, Ω_1 is the amplitude of the spindle speed, and $\omega_m = 2\pi/T$ is the angular modulation frequency. In practice, $\Omega_1 < 0.2\Omega_0$.

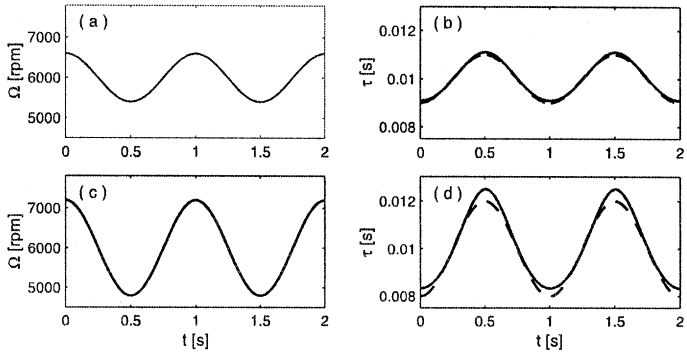

Figure 3. Spindle speed modulations with the corresponding exact (solid line) and approximated (dashed line) delays for $\Omega_0 = 6000$ rpm, $T = 1$ s, $\Omega_1 = 0.1\Omega_0$ (a, b) and $\Omega_1 = 0.2\Omega_0$ (c, d).

The exact time delay variation can be determined by solving equation (19) for $\tau(t)$. For the cosine type spindle speed modulation defined by equation (20), the integration in equation (19) yields the implicit equation

$$\frac{1}{60}\left(\Omega_0\tau(t) + \frac{1}{\omega_m}\Omega_1\left(\sin(\omega_m t) - \sin\left(\omega_m\left(t - \tau(t)\right)\right)\right)\right) = 1. \tag{21}$$

In this case, the function $\tau(t)$ cannot be given in closed form; it can only be computed numerically. Still, if Ω_1 is small enough, then the approximation

$$\tau(t) \approx \tau_0 - \tau_1 \cos(\omega_m t) \tag{22}$$

can effectively be used, where $\tau_0 = 60/\Omega_0$ and $\tau_1/\tau_0 = \Omega_1/\Omega_0$. In Figure 3, the exact time delays obtained by the numerical solution of equation (21) and the approximate time delays determined by equation (22) are compared for 10% and 20% spindle speed modulation. The maximum deviation between the exact and the approximated delays are 0.9% for 10% modulation (see Figure 3(b)) and 4% for 20% modulation (see Figure 3(d)). In the analysis below, equation (22) will be used as an expression for the delay variation.

Introducing the dimensionless time $\tilde{t} = \omega_n t$ gives the dimensionless equation of motion

$$\ddot{x}(\tilde{t}) + 2\zeta\dot{x}(\tilde{t}) + x(\tilde{t}) = \tilde{w}\left(x(\tilde{t} - \tilde{\tau}(\tilde{t})) - x(\tilde{t})\right), \tag{23}$$

where $\tilde{w} = Kw/\left(m\omega_n^2\right)$ is considered to be a kind of dimensionless (or normalized) depth of cut, and $\tilde{\tau}(\tilde{t}) = \tilde{\tau}_0 - \tilde{\tau}_1 \cos\left(\tilde{\omega}_m\tilde{t}\right)$ is the dimensionless time delay. Here, $\tilde{\tau}_0 = \omega_n\tau_0$ is the dimensionless mean delay, $\tilde{\tau}_1 = \omega_n\tau_1$ is the dimensionless delay amplitude, and $\tilde{\omega}_m = \omega_m/\omega_n$ is the dimensionless modulation frequency.

In the subsequent analysis, the stability charts will be determined in the plane of the dimensionless (or normalized) mean spindle speed $\tilde{\Omega}_0 = \Omega_0/(60f_n)$ and the dimensionless depth of cut $\tilde{w}$. Here $f_n = \omega_n/2\pi$ is the natural frequency of the tool and, consequently,

$\tilde{\tau}_0 = 2\pi/\tilde{\Omega}_0$. The dimensionless modulation parameters are the ratio of the modulation period and the mean time delay

$$R_P = T/\tau_0 = 2\pi/(\omega_m \tau_0) = 2\pi/(\tilde{\omega}_m \tilde{\tau}_0), \tag{24}$$

and the modulation amplitude ratio

$$R_A = \tau_1/\tau_0 = \tilde{\tau}_1/\tilde{\tau}_0. \tag{25}$$

4. DETERMINATION OF STABILITY CHARTS BY SEMIDISCRETIZATION METHOD

As the first step of the semidiscretization of equation (23), the approximation parameter k should be chosen and the time-step should be defined as

$$\Delta\tilde{t} = \tilde{t}_{i+1} - \tilde{t}_i = \frac{\tilde{T}}{k} = \frac{R_P \tilde{\tau}_0}{k} = \frac{2\pi R_P}{k\tilde{\Omega}_0}. \tag{26}$$

The integers m_i can be determined according to equation (3)

$$m_i = \operatorname{int}\left(\frac{\tilde{\tau}_i + \Delta\tilde{t}/2}{\Delta\tilde{t}}\right) = \operatorname{int}\left(\frac{k(1 - R_A c_i)}{R_P} + \frac{1}{2}\right), \tag{27}$$

since

$$\frac{\tilde{\tau}_i}{\Delta\tilde{t}} = \frac{\tilde{\tau}_0 - \tilde{\tau}_1 c_i}{\Delta\tilde{t}} = \frac{\tilde{\tau}_0}{\Delta\tilde{t}}\left(1 - \frac{\tilde{\tau}_1}{\tilde{\tau}_0} c_i\right) = k\frac{\tilde{\tau}_0}{\tilde{T}}(1 - R_A c_i) = \frac{k(1 - R_A c_i)}{R_P}, \tag{28}$$

where

$$c_i = \frac{k}{2\pi}\int_{i2\pi/k}^{(i+1)2\pi/k} \cos(\tilde{t})\mathrm{d}\tilde{t}. \quad i = 0, \ldots, k-1. \tag{29}$$

The maximum integer M is defined now as in equation (4).

Equation (23) is transformed to the form

$$\dot{\mathbf{x}}(\tilde{t}) = \mathbf{A}\mathbf{x}(\tilde{t}) + \mathbf{B}\mathbf{x}(\tilde{t} - \tilde{\tau}(\tilde{t})), \tag{30}$$

where

$$\mathbf{A} = \begin{pmatrix} 0 & 1 \\ -(1+\tilde{w}) & -2\zeta \end{pmatrix}, \quad \mathbf{B} = \begin{pmatrix} 0 & 0 \\ \tilde{w} & 0 \end{pmatrix}, \quad \mathbf{x}(\tilde{t}) = \begin{pmatrix} x(\tilde{t}) \\ \dot{x}(\tilde{t}) \end{pmatrix}. \tag{31}$$

Here, unlike in equation (1), the coefficient matrices **A** and **B** are not time-dependent. Consequently, the discretized equation is defined as

$$\dot{\mathbf{x}}(\tilde{t}) = \mathbf{A}\,\mathbf{x}(\tilde{t}) + \mathbf{B}\,\mathbf{x}_{\tilde{\tau}_i}, \quad \tilde{t} \in [\tilde{t}_i, \tilde{t}_{i+1}], \tag{32}$$

where

$$\mathbf{x}_{\tilde{\tau}_i} = \beta_i\,\mathbf{x}_{i-m_i} + \alpha_i\,\mathbf{x}_{i-m_i+1}, \tag{33}$$

and, using equations (8), (9), and (28), the weights are

$$\beta_i = \frac{k(1 - R_A c_i)}{R_P} + \frac{1}{2} - m_i, \tag{34}$$

$$\alpha_i = m_i + \frac{1}{2} - \frac{k(1 - R_A c_i)}{R_P}. \tag{35}$$

According to equation (12), $\mathbf{x}_{i+1}$ is defined as

$$\mathbf{x}_{i+1} = \mathbf{P}\mathbf{x}_i + \alpha_i \mathbf{R}\mathbf{x}_{i-m_i+1} + \beta_i \mathbf{R}\mathbf{x}_{i-m_i}, \tag{36}$$

where

$$\mathbf{P} = \exp\left(\mathbf{A}\Delta\tilde{t}\right) = \begin{pmatrix} P_{11} & P_{12} \\ P_{21} & P_{22} \end{pmatrix},$$

$$\mathbf{R} = \left(\exp\left(\mathbf{A}\Delta\tilde{t}\right) - \mathbf{I}\right)\mathbf{A}^{-1}\mathbf{B} = \begin{pmatrix} R_{11} & 0 \\ R_{21} & 0 \end{pmatrix}.$$

Note that the second column of matrix **B** is zero and, consequently, the second column of matrix **R** is also zero. This is because in equation (23) the derivatives of the delayed terms such as $\dot{x}(\tilde{t} - \tilde{\tau}(\tilde{t}))$ do not occur. Consequently, $\mathbf{x}_{i+1}$ depends on x_i, $\dot{x}_i$, x_{i-m_i+1} and x_{i-m_i}, but it does not depend on $\dot{x}_{i-m+1}$ and $\dot{x}_{i-m}$. This means that for the discrete map the $(M+2)$-dimensional state vector

$$\mathbf{z}_i = \mathrm{col}(x_i \;\; \dot{x}_i \;\; x_{i-1} \;\; \ldots \;\; x_{i-M}) \tag{37}$$

can be defined instead of the $n(M+1) = 2(M+1)$-dimensional vector

$$\mathbf{y}_i = \mathrm{col}(\mathbf{x}_i \;\; \mathbf{x}_{i-1} \;\; \ldots \;\; \mathbf{x}_{i-M}) = \mathrm{col}(x_i \;\; \dot{x}_i \;\; x_{i-1} \;\; \dot{x}_{i-1} \;\; \ldots \;\; x_{i-M} \;\; \dot{x}_{i-M}) \tag{38}$$

given by equation (14). This trick makes the size of the resulted discrete map much smaller

$$\mathbf{z}_{i+1} = \mathbf{D}_i \mathbf{z}_i, \tag{39}$$

where the $(M+2)$-dimensional coefficient matrix reads

$$\mathbf{D}_i = \begin{pmatrix} P_{11} & P_{12} & 0 & 0 & \dots & 0 & \alpha_i R_{11} & \beta_i R_{11} & 0 & \dots & 0 & 0 & 0 \\ P_{21} & P_{22} & 0 & 0 & \dots & 0 & \alpha_i R_{21} & \beta_i R_{21} & 0 & \dots & 0 & 0 & 0 \\ 1 & 0 & 0 & 0 & \dots & 0 & 0 & 0 & 0 & \dots & 0 & 0 & 0 \\ 0 & 0 & 1 & 0 & \dots & 0 & 0 & 0 & 0 & \dots & 0 & 0 & 0 \\ \vdots & \vdots & \vdots & \ddots & \ddots & \vdots & \vdots & \vdots & \vdots & \vdots & \vdots & \vdots & \vdots \\ & & & & & & & & & & & & \\ \vdots & \vdots & \vdots & \vdots & \vdots & \vdots & \vdots & \vdots & \ddots & \ddots & \vdots & \vdots & \vdots \\ 0 & 0 & 0 & 0 & \dots & 0 & 0 & 0 & 0 & \ddots & 0 & 0 & 0 \\ 0 & 0 & 0 & 0 & \dots & 0 & 0 & 0 & 0 & \dots & 1 & 0 & 0 \\ 0 & 0 & 0 & 0 & \dots & 0 & 0 & 0 & 0 & \dots & 0 & 1 & 0 \end{pmatrix}. \tag{40}$$

Here, $\alpha_i R_{11}$ and $\beta_i R_{11}$ are the (m_i+1)th and (m_i+2)th elements in the first row and $\alpha_i R_{21}$ and $\beta_i R_{21}$ are the (m_i+1)th and (m_i+2)th elements in the second row of matrix $\mathbf{D}_i$.

The transition matrix $\mathbf{\Phi}$ over the principal period $\tilde{T} = k\Delta\tilde{t}$ is determined now by coupling equations (39) for $i = 0, 1, \dots, k-1$:

$$\mathbf{\Phi} = \mathbf{D}_{k-1}\mathbf{D}_{k-2}\dots\mathbf{D}_1\mathbf{D}_0. \tag{41}$$

If the eigenvalues μ_i, $i = 1, \dots, M+2$ of $\mathbf{\Phi}$ are in modulus less than one, then the system is stable. Stability charts can be derived by evaluation of the transition matrix and the corresponding critical eigenvalue for a grid of different spindle speeds and depths of cut.

Based on the above algorithm, a Matlab code is given in the Appendix for the stability chart construction via the semidiscretization method.

The semidiscretization method can also be used to determine time history; if matrices $\mathbf{D}_i$ are known for $i = 0, \dots, k-1$, then the vibration signal can be computed by the recursive formula (39) using the first elements of each $\mathbf{z}_i$. The initial values (actually, the approximate initial function for the VDDE) are given by $\mathbf{z}_0$ for this simulation via semidiscretization.

5. CHATTER FREQUENCIES

The chatter frequencies for unstable cutting processes are also determined by one of the critical characteristic multipliers μ_1, where $|\mu_1| \geq |\mu_i|$, $i = 2, 3, \dots, M+2$. The critical characteristic multipliers are located in three possible ways (see Figure 4).

1. They are a complex pair ($\mu_1 = \bar{\mu}_2$) located on the unit circle ($|\mu_{1,2}| = 1$). This case is topologically equivalent to the primary Hopf bifurcation of autonomous systems and called a secondary Hopf or Neimark–Sacker bifurcation. The corresponding motion is quasi-periodic.
2. $\mu_1 = 1$. The associated bifurcation is topologically equivalent to the saddle-node bifurcation of autonomous systems and is called a period-one bifurcation. The corresponding motion is $\tilde{T}$-periodic.

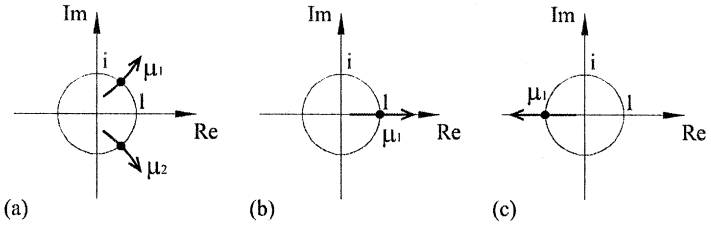

Figure 4. Critical characteristic multipliers: secondary Hopf (a), period-one (b), and period-two (c) bifurcations.

3. $\mu = -1$. There is no topologically equivalent type of bifurcation for autonomous systems. This case is called period two, period doubling, or flip bifurcation. The corresponding motion is $2\tilde{T}$-periodic.

At this point, it should be emphasized that different chatter types are distinguished according to the principal period. For turning with varying spindle speed, the principal period is the spindle speed modulation period as opposed to the case of milling with constant spindle speed, where the principal period is the tooth passing period.

If $\tilde{\gamma}_1 = \mathrm{Im}(\ln \mu_1)$ denotes the polar angle of the critical characteristic multiplier with the restriction $\tilde{\gamma}_1 \in [0, 2\pi)$, then the arising chatter frequencies are

$$\tilde{f} = \left\{ \frac{\pm\tilde{\gamma}_1 + h2\pi}{\tilde{T}} \right\}, \quad h = 0, 1, \ldots, \tag{42}$$

where the sign $\pm$ refers to the case when the critical characteristic multiplier is a complex pair, and the complex conjugate should also be considered. Of course, only the positive values of these frequencies have physical meaning.

If $\mu_1 = 1$ (the case of period-one bifurcation), then $\tilde{\gamma}_1 = \mathrm{Im}(\ln(1)) = 0$, and the frequencies are multiples of the modulation frequency:

$$\tilde{f} = \frac{h2\pi}{\tilde{T}}, \quad h = 0, 1, \ldots . \tag{43}$$

If $\mu_1 = -1$ (the case of period-two bifurcation), then $\tilde{\gamma}_1 = \mathrm{Im}(\ln(-1)) = \pi$, and the frequencies are

$$\tilde{f} = \frac{\pi + h2\pi}{\tilde{T}}, \quad h = 0, 1, \ldots . \tag{44}$$

For turning with constant spindle speed, primary Hopf bifurcation is the only possible route to lose stability. For milling (with constant spindle speed), secondary Hopf and period-two (or flip) bifurcations can occur, but the period-one bifurcation is excluded (see Davies et al., 2002; Insperger et al., 2003). For turning with varying spindle speed, all three cases (the period-one, period-two, and secondary Hopf bifurcations) arise at different parts of the stability boundary.

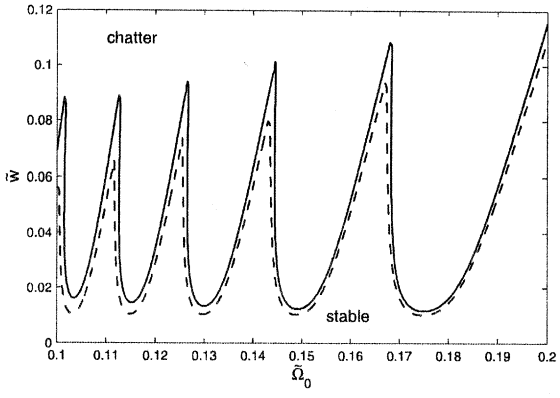

Figure 5. Stability boundaries for turning with varying spindle speed (solid lines) and with constant spindle speed (dashed lines). The parameters $\zeta = 0.005$, $R_A = 0.02$, and $R_P = 0.4$ are taken from Pakdemirli and Ulsoy (1997).

The chatter frequencies are often compared to the modulation frequency and to its harmonics. The modulation frequency and its harmonics are inversely proportional to the modulation period, and therefore linearly proportional to the dimensionless spindle speed:

$$\tilde{f}_m = \frac{h2\pi}{\tilde{T}} = \frac{h\tilde{\Omega}_0}{R_P}, \quad h = 1, 2, \ldots : \tag{45}$$

Note that in the case of period-one bifurcation ($\mu_1 = 1$), the chatter frequencies are equal to the modulation frequencies. In the case of period-two bifurcation ($\mu_1 = -1$), the lowest frequency among the harmonics is half of the basic modulation frequency.

6. COMPARISON WITH PREVIOUS RESULTS

Two examples are chosen to be compared to the stability charts obtained by semidiscretization. First, the stability chart obtained by Pakdemirli and Ulsoy (1997) is considered. The parameters are $\zeta = 0.005$ and $R_A = 0.02$. Pakdemirli and Ulsoy (1997) used a fixed modulation period; the corresponding average modulation period ratio was $R_P = 0.375$. Since the modulation amplitude ratio is small, they used a perturbation technique to derive stability chart. They obtained a slight improvement in stability by using varying spindle speeds.

The stability chart derived by semidiscretization is presented in Figure 5. This result is practically identical to that of Pakdemirli and Ulsoy (1997). Since the modulation period ratio is quite small, the differences between the stability boundaries of turning with constant and varying spindle speed are small. As can be seen, the improvement in stability slightly increases for lower spindle speeds.

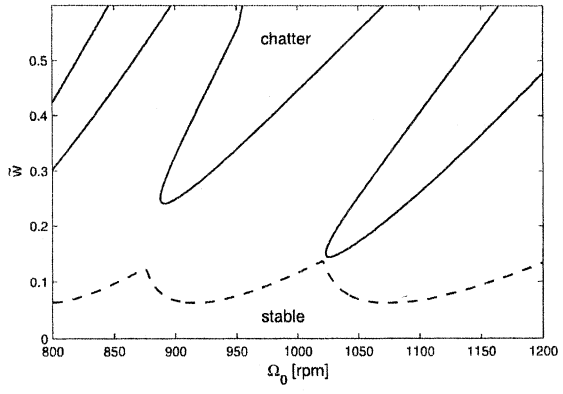

Figure 6. Stability boundaries for turning with varying spindle speed (solid lines) and with constant spindle speed (dashed lines). The parameters $f_n = 100$ Hz, $\zeta = 0.03$, $R_A = 0.25$, and $R_P = 0.4$ are taken from Jayaram et al. (2000).

The other example is the chart obtained by Jayaram et al. (2000) (see Figure 8 in their paper). They assumed a 1DOF system with natural frequency $f_n = 100$ Hz and damping ratio $\zeta = 0.03$. The modulation parameters were $R_A = 0.25$ and $R_P = 0.4$. They used quasi-periodic trial solutions for the VDDE, combined the Fourier expansion with Bessel functions, and determined stability boundaries by harmonic balance.

The stability chart constructed by semidiscretization for these parameters is presented in Figure 6. This chart differs substantially from the stability chart of Jayaram et al. (2000). The explanation of this difference calls attention to a new phenomenon in the stability charts of time-varying cutting. In conventional turning, there is a unique connection between the spindle speed and critical depth of cut. For time-varying cutting, the critical depth of cut is not unique, stable and unstable domains alternate along the depth of cut. Jayaram et al. (2000) calculated some of the stability limit points correctly, but only one (usually, the minimal) critical depth of cut was determined for each spindle speed. Therefore, the continuous connection of these points in their stability chart was optional and sometimes misleading. Recently, having known the stability charts of high-speed milling with time-varying cutting coefficients (Insperger and Stépán, 2000; Mann et al., 2003; Szalai and Stépán, 2003), the appearance of the slant stability lobes is not surprising here either.

Note that both reference cases used extremely high modulation frequency (more than double the spindle rotation frequency). These are hardly realizable on conventional industrial turning lathes. In the next section, we investigate turning with more realistic modulation parameters.

7. STABILITY CHARTS

Stability charts and the associated chatter frequencies were determined for modulation amplitude ratio $R_A = 0.1$ and for modulation period ratios $R_P = 2$, 5, 10, and 20. The lobes

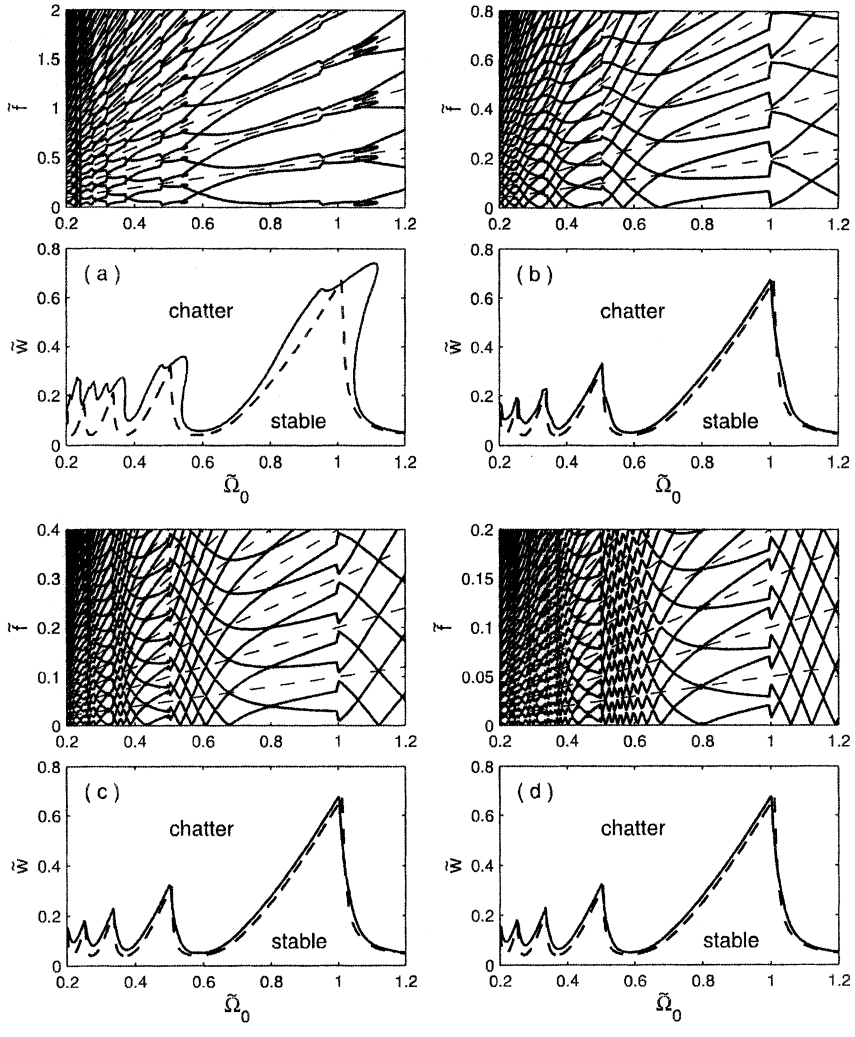

Figure 7. Stability charts and chatter frequencies for turning with varying spindle speeds (solid lines) with modulation parameters $R_A = 0.1$ and $R_P = 2$ (a), $R_P = 5$ (b), $R_P = 10$ (c), $R_P = 20$ (d), and stability boundaries for turning without speed modulation (dashed lines).

and the frequencies are shown in Figure 7. Note that dimensionless spindle speed and dimensionless depth of cut are used as technological parameters. The damping was set to $\zeta = 0.02$ for all the charts.

During the computations, the approximation parameter was $k = 40R_P$. With $R_A = 0.1$, this resulted in $M = 44$. For example, if $R_P = 10$, then $k = 400$ pieces of 46×46 dimensional matrices should be multiplied to obtain the transition matrix $\mathbf{\Phi}$ according to equation (41). For these approximation parameters, the difference between the exactly

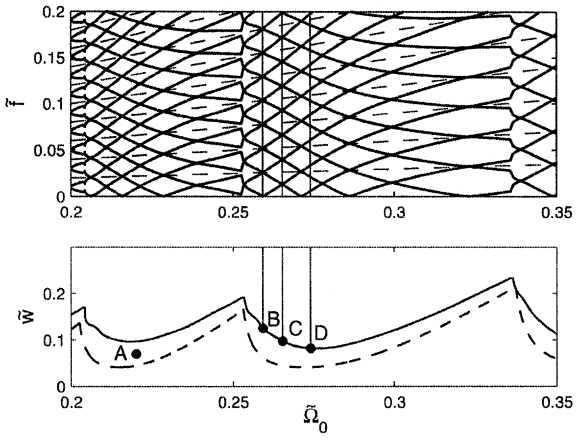

Figure 8. Stability charts and chatter frequencies for $R_A = 0.1$ and $R_P = 10$.

known stability lobes of conventional (constant speed) turning and those obtained by the semidiscretization method with $R_A = 0$ was less than 1% in the presented parameter domain ($\tilde{\Omega}_0 = 0.2$–1.2 and $\tilde{w} = 0$–0.8).

First, we check the high-speed domain. As can be seen, the most significant improvement in stability was achieved by modulation period ratio $R_P = 2$. As this ratio increases, the system can be considered quasi-autonomous, and the charts converge to those of conventional turning with constant spindle speed. Since the modulation period ratio $R_P = 2$ is hardly achievable on turning lathes, especially for the high-speed regime, the stability improvement shown by chart (a) in Figure 7 is not likely to be used in practice in the near future.

For low spindle speed domain, a slight improvement in stability can be observed also for large R_P values. A zoomed stability chart for $R_A = 0.1$ and $R_P = 10$ is shown in Figure 8. Point A in Figure 8 is associated with dimensionless spindle speed $\tilde{\Omega}_0 = 0.22$ and dimensionless depth of cut $\tilde{w} = 0.07$. The simulated time histories obtained via semidiscretization for turning with constant and varying ($R_A = 0.1$, $R_P = 10$) spindle speeds are shown in Figure 9 for the parameters determined by point A. It can be seen that without speed modulation, the turning process is unstable (chatter arise), while spindle speed modulation stabilizes the process.

The arising frequencies are also plotted above the charts. Since the speed modulation is periodic, a whole set of chatter frequencies occurs, as described by equation (42). It can be observed in Figure 7 that the larger the modulation period R_P is, the lower the chatter frequencies are. This is due to the fact that the chatter frequencies are in connection with the modulation period according to equation (42). The modulation frequency and its harmonics given by equation (45) are presented by dashed lines in the frequency plots. At the points, where the chatter frequencies (thick curves) intersect these dashed lines, the transition matrix $\mathbf{\Phi}$ has an eigenvalue equal to 1, i.e. period-one bifurcation occurs. At the points where the chatter frequency curves intersect each other in the middle between two neighboring dashed

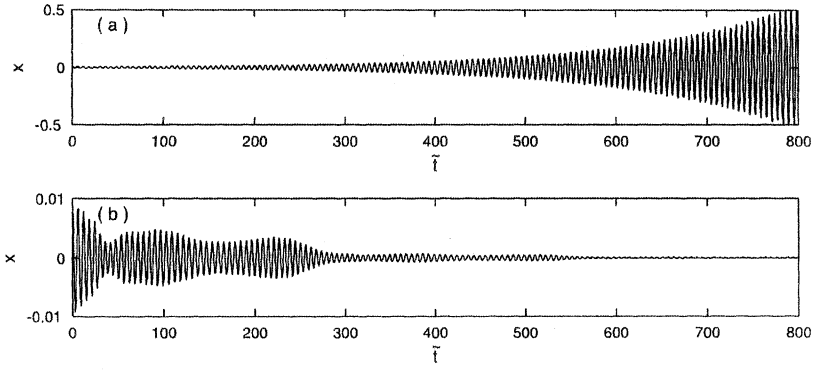

Figure 9. Time histories for cutting at point A in Figure 8 with constant spindle speed $R_A = 0$ (a) and with varying spindle speed $R_A = 0.1$ (b).

lines, the transition matrix $\mathbf{\Phi}$ has an eigenvalue equal to -1, i.e. period-two bifurcation occurs. Note that these bifurcations are not the same as those of conventional (constant speed) turning and milling processes. The difference is that for turning with spindle speed variation, the bifurcations are related to the spindle speed modulation period $\tilde{T}$, while for conventional turning or milling, they are related to the spindle speed period or to the tooth pass period, respectively. For turning with spindle speed variation, period-one and period-two motions mean that the tool vibration is $\tilde{T}$- and $2\tilde{T}$-periodic, respectively.

Points B, C, and D in Figure 8 are related to period-one, period-two and secondary Hopf bifurcations, respectively. At point B, $\tilde{\Omega}_0 = 0.2592$, $\tilde{w} = 0.1249$; at point C, $\tilde{\Omega}_0 = 0.2653$, $\tilde{w} = 0.0977$; at point D, $\tilde{\Omega}_0 = 0.274$, $\tilde{w} = 0.0819$.

The continuous and $1/\tilde{T}$-sampled time histories, the Poincaré sections, and the power spectra are shown in Figure 10. In the power spectra plots, dashed lines denote the modulation frequency and its harmonics, as given in equation (45). The period-one and the period-two cases can be distinguished by the $1/\tilde{T}$-sampled black dots. For cutting at B, the motion is $\tilde{T}$-periodic, and it is presented as a point in the Poincaré section. For cutting at C, the $1/\tilde{T}$-sampled signal changes sign alternately for each sample (see the black dots). This corresponds to the period-two motion associated with the characteristic multiplier $\mu_1 = -1$. For this case, the motion is presented as two points in the Poincaré section. For cutting at D, the motion is quasi-periodic associated with a secondary Hopf bifurcation; consequently, the points of the Poincaré section form a circle.

8. CONCLUSIONS

We have investigated a 1DOF model of turning with varying spindle. The corresponding VDDE was analyzed by the semidiscretization method. The method was introduced for a general VDDE and it was applied for the turning process. The code for the stability chart construction is given in the Appendix.

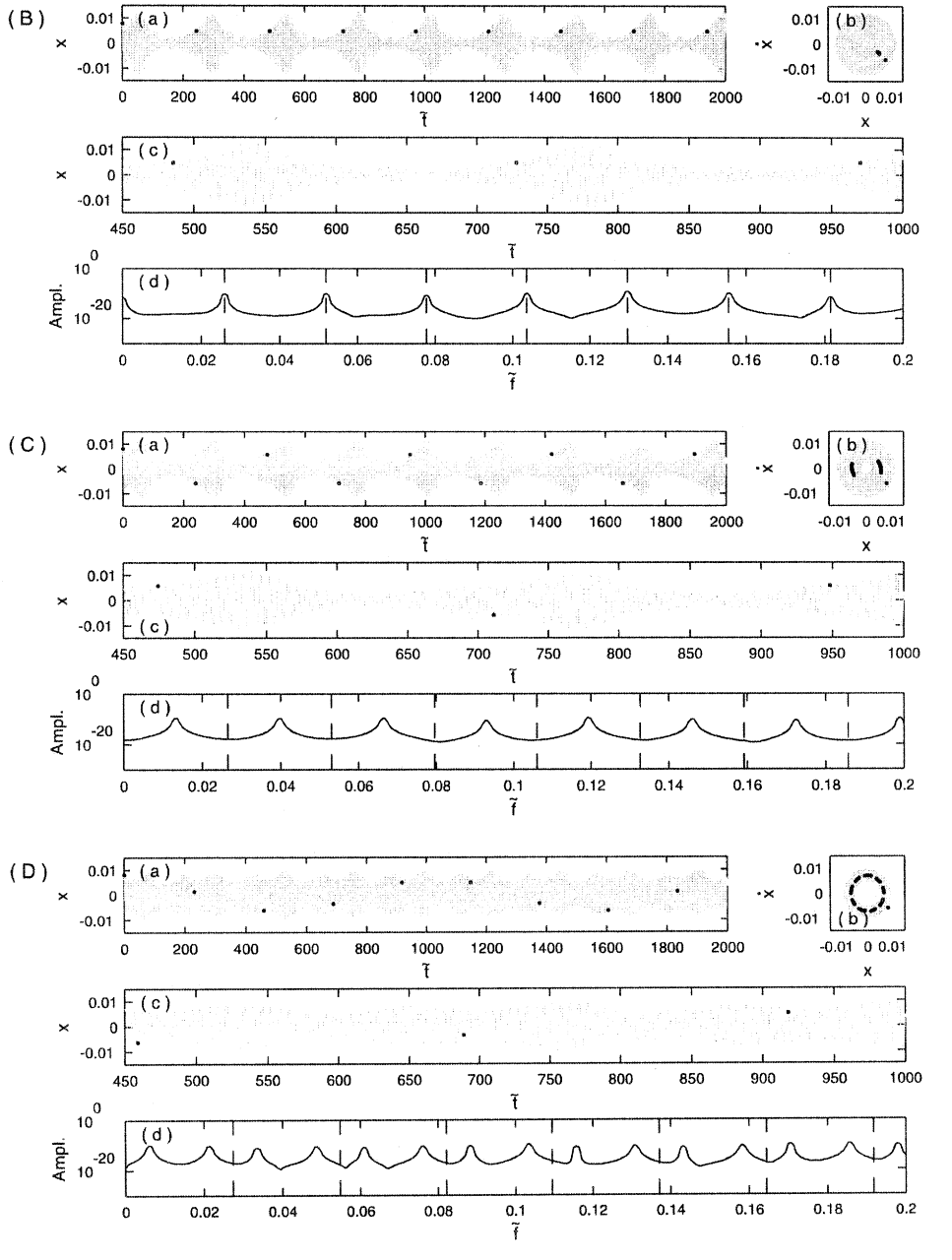

Figure 10. Continuous and $1/\tilde{T}$-sampled time histories (a), Poincaré section (b), zoomed time histories (c), and power spectra for cutting at points B, C, and D in Figure 7.

We compared the turning process with constant and with varying spindle speeds. The technological parameters were non-dimensionalized (normalized). Different modulation periods were analyzed, while the modulation amplitude was set to the reasonable value of 10%. It was found that for certain cases a higher depth of cut values and, consequently, higher material removal rates are possible if the spindle speed is modulated. The stabilization effect was found to be stronger for small modulation periods. Comparing the high- and low-speed domains, it was found that spindle speed variation with a reasonable modulation period ($R_P \geq 10$) results in no essential changes in the high-speed domain, but it definitely results in a significant improvement in stability for low speeds.

The most significant improvement in stability was achieved by modulation period ratio $R_P = 2$. For turning lathes, this ratio is practically not realizable with the available technical solutions at the moment, especially for the high-speed regime.

Analysis of the chatter frequencies and the corresponding characteristic multipliers showed that in addition to secondary Hopf and period-two bifurcations (which are typical for milling process), period-one bifurcation is also a possible way of losing stability in the case of turning with varying spindle speed. Continuous and sampled chatter signals, Poincaré sections, and power spectra were determined numerically for the three cases: the period-one, the period-two, and the secondary Hopf bifurcations.

APPENDIX A: MATLAB CODE FOR THE DELAYED MATHIEU EQUATION

```
clear
% parameters
R_P=10;                                  % modulation period ratio
R_A=0.1;                                 % modulation amplitude ratio
zeta=0.02;                               % damping
step_o=200;                              % number of steps for spindle speed Ω̃
step_w=150;                              % number of steps for depth of cut w̃
o_start=0.2;                             % starting value for Ω̃
o_end=1.2;                               % final value for Ω̃
o_step=(o_end-o_start)/step_o;
w_start=0;                               % starting value for w̃
w_end=0.8;                               % final value for w̃
w_step=(w_end-w_start)/step_w;
% computational parameters
k=40*R_P;                                % approximation parameter
syms t
for i=1:k
    c_i = k/(2*pi)*quadl('cos(t)',(i-1)*2*pi/k,(i)*2*pi/k);   % integration of c_i
    m(i)=floor(k/R_P*(1-R_A*c_i)+1/2);                        % determination of m_i
    beta(i)=k*(1-R_A*c_i)/R_P +1/2 -m(i);                     % determination of α_i
    alpha(i)=m(i)+1/2-k*(1-R_A*c_i)/R_P;                      % determination of β_i
end
```

```
M=max(m)                                    % determination of M
A=zeros(2,2); A(1,2)=1; A(2,2)=-2*zeta;
B=zeros(2,2);
D=zeros(M+2,M+2);
d=ones(M+1,1); d(1:2)=[0 0];
D=D+diag(d,-1); D(3,1)=1;
% start of computation
i=0;
for y=1:step_w+1                            % loop for w̃
    w=w_start+(y-1)*w_step;
    for x=1:step_o+1                        % loop for Ω̃
        o=o_start+(x-1)*o_step;
        T=2*pi*R_P/o;                       % T̃
        dt=T/k;                             % Δt̃
        A(2,1)=-(1+w);                      % matrix A
        B(2,1)=w;                           % matrix B
        P=expm(A*dt);                       % matrix P
        R=(expm(A*dt)-eye(2))*inv(A)*B;     % matrix R
        D(1:2,1:2) = P;                     % matrix D_i
        Fi = eye(M+2,M+2);
        for i=1:k
            D(1:2,m(i)+1) = alpha(i)*R(1:2,1:1);        % matrix D_i
            D(1:2,m(i)+2) = beta(i)*R(1:2,1:1);         % matrix D_i
            Fi = D*Fi;                                  % Floquet transition matrix Φ
            D(1:2,m(i)+1) = [0 0]';                     % matrix D_i
            D(1:2,m(i)+2) = [0 0]';                     % matrix D_i
        end
        ss(x,y)=o;                          % matrix of spindle speeds
        dc(x,y)=w;                          % matrix of depth of cuts
        ei(x,y)=max(abs(eig(Fi)));          % matrix of eigenvalues
    end
    step_w+1-y                              % counter
end
figure
contour(ss,dc,ei,[1, 1],'k')
```

Acknowledgments. This research was supported in part by the Magyary Zoltán Postdoctoral Fellowship of Foundation for Hungarian Higher Education and Research, by the Hungarian National Science Foundation under grant no. OTKA T043368 and F047318, and the Research Group on Dynamics of Machines and Vehicles, Hungarian Academy of Sciences.

REFERENCES

Altintas, Y., Engin, S., and Budak, E., 1999, "Analytical stability prediction and design of variable pitch cutters," *Journal of Manufacturing Science and Engineering* **121**, 173–178.

Bayly, P. V., Halley, J. E., Mann, B. P., and Davies, M. A., 2003, "Stability of interrupted cutting by temporal finite element analysis," *Journal of Manufacturing Science and Engineering* **125** (2), 220–225.

Davies, M. A., Pratt, J. R., Dutterer, B., and Burns, T. J., 2002, "Stability prediction for low radial immersion milling," *Journal of Manufacturing Science and Engineering* **124** (2), 217–225.

Farkas, M., 1994, *Periodic Motions*, Springer-Verlag, NY.

Gouskov, A. M., Voronov, S. A., Paris, H., and Batzer, S. A., 2002, "Nonlinear dynamics of a machining system with two interdependent delays," *Communications in Nonlinear Science and Numerical Simulation* **7** (4), 207–221.

Gradišek, J., Friedrich, R., Govekar, E., and Grabec, I., 2002, "Analysis of data from periodically forced stochastic processes," *Physics Letters A* **294** (3–4), 234–238.

Győri, I., Hartung, F., and Turi, J., 1993, "Approximation of functional differential equations with time- and state-dependent delays by equations with piecewise constant arguments," *IMA Preprint Series* 1130.

Győri, I., Hartung, F., Turi, J., 1995, "Numerical approximations for a class of differential equations with time- and state-dependent delays," *Applied Mathematics Letters* **8** (6), 19–24.

Hale, J. K. and Lunel, S. M. V., 1993, *Introduction to Functional Differential Equations*, Springer-Verlag, New York.

Hosho, T., Sakisaka, N, Moriyama, I. Sato, M., Higashimoto, A., Tokugana, T., and Takeyama, T., 1977, "Study for practical application of fluctuating speed cutting for regenerative chatter control," *Annals of the CIRP* **25** (1), 175–179.

Inamura, T. and Sata, T., 1974, "Stability analysis of cutting under varying spindle speed," *Annals of the CIRP* **23** (1), 119–120.

Insperger, T. and Horváth, R., 2000, "Pendulum with harmonic variation of the suspension point," *Periodica Polytechnica, Mechanical Engineering* **44** (1), 39–46.

Insperger, T. and Stépán, G., 2000, "Stability of high-speed milling," in *Proceedings of the ASME 2000 DETC, Symposium on Nonlinear Dynamics and Stochastic Mechanics*, Orlando, FL, AMD-241, 119–123.

Insperger T. and Stépán, G., 2002, "Semidiscretization method for delayed systems," *International Journal for Numerical Methods in Engineering* **55** (5), 503–518.

Insperger, T., Stépán, G., and Namachchivaya, S., 2001, "Comparison of the dynamics of low immersion milling and cutting with varying spindle speed," in *Proceedings of the ASME 2001 Design Engineering Technical Conferences*, Pittsburgh, PA, paper no. DETC2001/VIB-21616 (CD-ROM).

Insperger, T., Mann, B. P., Stépán, G., and Bayley, P. V., 2003, "Stability of up-milling and down-milling, part 1: alternative analytical methods," *International Journal of Machine Tools and Manufacture* **43** (1), 25–34.

Jayaram, S., Kapoor, S. G., and DeVor, R. E., 2000, "Analytical stability analysis of variable spindle speed machining," *Journal of Manufacturing Science and Engineering* **122** (3), 391–397.

Kudinov, V. A., 1967, *Dynamics of Tool-Lathe*, Mashinostroenie, Moscow (in Russian).

Lakshmikantham, V. and Trigiante, D, 1988, *Theory of Difference Equations, Numerical Methods and Applications*, Academic Press, London.

Mann, B. P., Insperger, T., Bayly, P. V., and Stépán, G., 2003, "Stability of up-milling and down-milling, part 2: experimental verification", *International Journal of Machine Tools and Manufacture* **43** (1), 35–40.

Moon, F.C., 1998, *Dynamics and Chaos in Manufacturing Processes*, Wiley, NY.

Namachchivaya, N. S. and Beddini, R., 2003, "Spindle speed variation for the suppression of regenerative chatter," *Journal of Nonlinear Science* **13** (3), 265–288.

Pakdemirli, M. and Ulsoy, A. G., 1997, "Perturbation analysis of spindle speed variation in machine tool chatter," *Journal of Vibration and Control* **3**, 261–278.

Sastry, S., Kapoor, S. G., DeVor, R. E., and Dullerud, G. E., 2001, "Chatter stability analysis of the variable speed face-milling process," *Journal of Manufacturing Science and Engineering* **123** (4), 537–546.

Schmitz, T., Medicus, K., and Dutterer, B., 2002, "Exploring once-per-revolution audio signal variance as a chatter indicator," *Machining Science and Technology* **6** (2), 207–225.

Segalman, D. J. and Butcher, E. A., 2000, "Suppression of regenerative chatter via impedance modulation," *Journal of Vibration and Control* **6**, 243–256.

Sexton, J. S., Milne, R. D., and Stone, B. J., 1977, "A stability analysis of single point machining with varying spindle speed," *Applied Mathematical Modelling* **1**, 310–318.

Stépán, G., 1989, *Retarded Dynamical Systems*, Longman, Harlow.

Szalai, R. and Stépán, G., 2003, "Stability boundaries of high-speed milling corresponding to period doubling are essentially closed curves," in *Proceedings of ASME International Mechanical Engineering Conference and Exposition*, Washington, DC, paper no. IMECE2003-42122 (CD-ROM).

Takemura, T., Kitamura, T., Hoshi, T., and Okushima, K., 1974, "Active suppression of chatter by programmed variation of spindle speed", *Annals of the CIRP* **23** (1), 121–122.

Tlusty, J., Polacek, A., Danek, C., and Spacek, J., 1962, *Selbsterregte Schwingungen an Werkzeugmaschinen*, VEB Verlag Technik, Berlin.

Tobias, S. A., 1965, *Machine Tool Vibration*, Blackie, London.

Tsao, T. C., McCarthy, M. W., and Kapoor, S. G., 1993 "A new approach to stability analysis of variable speed machining systems," *International Journal of Machine Tools and Manufacture* **33** (6), 791–808.

Yilmaz, A., Al-Regib, E., and Ni, J., 2002, "Machine tool chatter suppression by multilevel random spindle speed variation," *Journal of Manufacturing Science and Engineering* **124** (2), 208–216.

Zhao, M. X. and Balachandran, B., 2001, "Dynamics and stability of milling process," *International Journal of Solids and Structures* **38** (10–13), 2233–2248.